Structural Roles of TiO_2 in CaF_2-SiO_2-CaO-TiO_2 Submerged Arc Welding Fluxes

Yanyun Zhang, Theresa Coetsee, Haifeng Yang, Tan Zhao & Cong Wang*

YANYUN ZHANG is with the School of Metallurgy, Northeastern University, Shenyang 110819, China.

THERESA COETSEE is with the Department of Materials Science and Metallurgical Engineering, University of Pretoria, Pretoria, 0002, South Africa.

HAIFENG YANG is with the Minmetals Yingkou Medium Plate Co., Ltd, Yingkou 115005, China.

TAN ZHAO is with the State Key Laboratory of Metal Material for Marine Equipment and Application, Angang Steel Co., Ltd, Anshan 114021, China.

CONG WANG is with the School of Metallurgy, Northeastern University and also with the State Key Laboratory of Rolling and Automation, Northeastern University, Shenyang 110819, China.

*Contact e-mail: wangc@smm.neu.edu.cn

Abstract

A series of fused CaF_2-SiO_2-CaO-based fluxes geared towards submerged arc welding has been prepared with incremental TiO_2 additions. Through systematic investigation on physical properties, quantitative relationship between TiO_2 content and corresponding structural information has been established, and the roles played by TiO_2 have been profiled. It is found that TiO_2 has been introduced into the silicate network by acting as network-former, increasing the degree of polymerization while lowering the strength of the flux.

Due to high efficiency, submerged arc welding (SAW) has been extensively applied in a wide spectrum of engineering settings, such as pressure vessel, oil and gas pipeline, offshore and shipbuilding.[1,2] For SAW operation, welding fluxes are designed to perform essential functions, including protecting the weld pool from oxidation, adding alloying elements to the weld metal (WM), refining weld pool, and improving welding efficacy.[3] As a matter of fact, such functions are enabled, to a large extent, by the physicochemical properties, namely, melting point, viscosity, thermal and electrical conductivity, and activity, of the fluxes, which, in turn, are inherently rooted in the structures.[4,5,6] Therefore, an illustrated understanding of the fine structure is of crucial significance for flux designing strategies geared towards various SAW applications.

Over the past decades, CaF_2-CaO-SiO_2 based fused fluxes, owing to satisfactory chemical homogeneity, non-hygroscopic nature, low oxygen potential, and fine arc stability, have been applied for SAW engineering of high strength low alloy (HSLA) steel grades.[2,7,8] Among them, TiO_2-bearing variants have also been developed for enhanced slag detachability as well as improved arc stability.[2] On top of these advantages, Ti-containing inclusions introduced into the weld pool *via* slag-metal reactions can promote the nucleation of acicular ferrites (AF),[9,10] which has been proven to be effective enhancing WM fracture toughness.[1,7] It

needs to be pointed out that controversies regarding the structural roles of TiO_2 and how Ti is transferred from the flux to the weld metal still persist, as pertinent analysis over flux structure evolution is far from complete.[10,11,12] Previous TiO_2 based studies mainly focused on blast furnace slag and mold slag, and to date, there has been debate about the structural roles of TiO_2 in slag. Shon *et al*.[13] and Shankar *et al*.[14] studied the effect of TiO_2 on the viscosity of $CaO\text{-}SiO_2\text{-}MgO\text{-}Al_2O_3\text{-}TiO_2$ mold slags, indicating that viscosity decreases with TiO_2 addition and TiO_2 serves primarily as network-breakers. On the contrary, Zheng *et al*.[15] showed that TiO_2 might be considered as network-formers in $CaO\text{-}SiO_2\text{-}TiO_2$ blast furnace slag system as it enhanced polymerization of the network. However, it needs to be pointed out that few investigations regarding the structures of $CaF_2\text{-}SiO_2\text{-}CaO\text{-}TiO_2$ welding flux system are available. In this regard, further investigations are called upon to account for the structural roles of TiO_2 in pertinent welding fluxes.

Quaternary $CaF_2\text{-}SiO_2\text{-}CaO\text{-}TiO_2$ system fused fluxes were designed and prepared through melting and quenching processes. Reagent grade chemicals of CaF_2, SiO_2, CaO, and TiO_2 (Produced by Sinopharm Chemical Reagent Co., Ltd) were employed. Before mixing, raw materials were preheated at 1073 K in the resistance furnace for 5 hours to remove any moisture. The mixed powders (1 kg) were smelted at 1823 K in a C-80 wt pct SiC crucible with an outer diameter of 18 cm and a height of 20 cm for 1 hour to ensure homogeneity, during which the crucible was sealed by a graphite cover to minimize evaporation of the fluoride species.[16] Subsequently, the molten flux was rapidly quenched in iced water (273 K). Quenched sample was then baked at 973 K for 3 hours to remove any residual graphite and moisture, and crushed into powders (< 74 μm) for structural characterization as well as physical measurements.

Chemical compositions analyses of the fluxes were carried out by X-ray fluorescence (XRF, ZXS Priums II, Rigaku). The XRF results of the pre-melted samples show that the carbon content is about 0.90 wt pct, which can be neglected in the subsequent analysis. The XRF analysis result of the fluxes is shown in Table I, in which the sample number represents corresponding nominal TiO_2 percentage, as negligible changes are found between nominal and analytical compositions. The total amounts of Ti^{3+} in the flux were determined by a modified version of an indirect potentiometric redox titration method. This method has a detection limit of approximately 10^{-6} moles of Ti^{3+} and an absolute error of ± 5 pct of the detected amount.[17] Table I shows that Ti^{3+} content was observed in the pre-melted samples. Therefore, only Ti^{4+}-related structural units are considered in the subsequent analysis.

The crystal structure of flux samples was characterized by powder X-ray diffraction (XRD, D8 Advance, Bruker). FTIR spectra were acquired using a spectrophotometer (Vertex 70, Bruker) equipped with KBr detector, with spectral region ranging from 4000 to 400 cm^{-1} at the resolution of 2 cm^{-1}. As for Raman spectra, a laser confocal Raman spectrometer (HR800, Horiba) was employed with an excitation wavelength of 488 nm and a light source of 1 mW semiconductor. X-ray photoelectron spectroscopy (XPS, ESCALAB 250Xi, Thermo Fisher) analysis was performed to measure O_{1s} binding energy on the surface, of which the results were calibrated by the C_{1s} binding energy at 284.5 eV.

Figure 1 shows XRD patterns of the fused flux samples. As can be seen, a unanimous yet diffusive pattern is found in the 2θ range of 20 to 40 deg, which demonstrates the amorphous nature of the fused fluxes. Such amorphous feature is indispensable for compositional

Table I. Chemical Compositions of the Fluxes (Wt Pct)

Sample No.	CaF_2	CaO	SiO_2	TiO_2	CaO/SiO_2	$Ti^{3+}/\Sigma Ti$
F0						
Design	25	37.5	37.5	0	1	—
Testing	24.08(± 2.43)	37.91(± 1.28)	38.01(± 2.18)	0.00	1.00	0
F5						
Design	25	35	35	5	1	—
Testing	24.28(± 2.46)	34.94(± 1.21)	36.12(± 2.07)	4.66(± 1.78)	0.97	0.01
F10						
Design	25	32.5	32.5	10	1	—
Testing	24.40(± 2.36)	32.38(± 1.18)	33.25(± 1.99)	9.97(± 1.91)	0.97	0.02
F15						
Design	25	30	30	15	1	—
Testing	24.28(± 2.50)	29.88(± 1.14)	30.65(± 1.98)	15.19(± 1.84)	0.97	0.03
F20						
Design	25	27.5	27.5	20	1	—
Testing	24.19(± 2.13)	27.50(± 1.13)	27.78(± 2.08)	20.53(± 1.81)	0.99	0.05

uniformity and potentially beneficial for weldability, as pointed out by Yu *et al.*[18] and Schwemmer *et al.*[19]

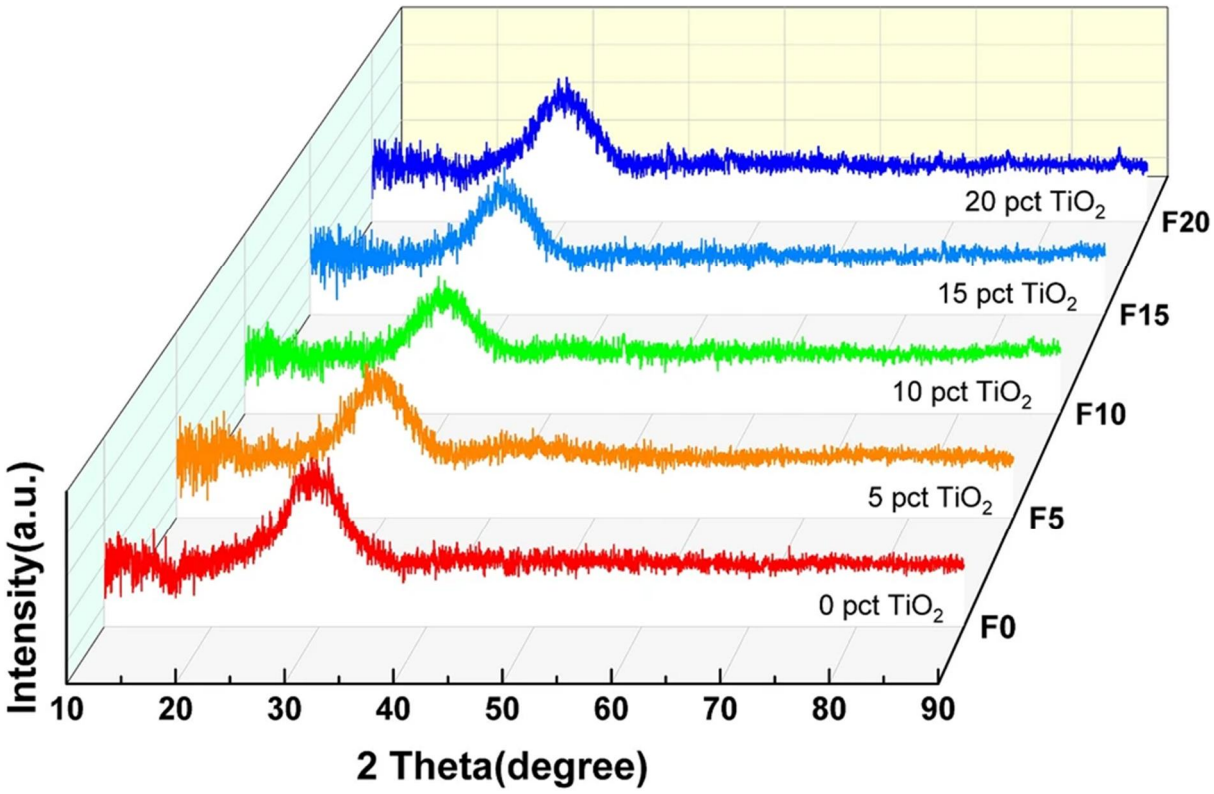

Fig. 1. XRD patterns of the fused flux samples

FTIR spectra of the amorphous flux samples are shown in Figure 2(a). As can be seen, all spectra exhibit three broad absorption bands: a high-frequency region from 800 to 1200 cm^{-1}, an intermediate-frequency region from 600 to 800 cm^{-1}, and a low-frequency region from 400 to 600 cm^{-1}.[20,21] The high-frequency region is related to the symmetric stretching vibrations bands of Si-O in [SiO_4]-tetrahedra silicate network.[22,23] Conventionally, the stoichiometric notations for five types of [SiO_4]-tetrahedra units in high-frequency region are defined as Q^i (i ranges from 0 to 4, and i represents the number of bridging oxygens in one [SiO_4]-tetrahedra),[24] wherein five types of units are $[SiO_4]^{4-}$ (Q^0, monomer), $[Si_2O_7]^{6-}$ (Q^1, dimmer), $[Si_2O_6]^{4-}$ (Q^2, chain), $[Si_4O_{11}]^{6-}$ (Q^3, sheet), and SiO_2 (Q^4, fully polymerized) groups, respectively.[25] The Q^0 to Q^4 are located at positions of ~850, ~900, 950 to 1000, ~1050, and ~1200 cm^{-1}, respectively.[26,27] These four types of Q^i bands are labeled in Figure 2(a), and Q^4 is not observed in any samples due to its very low intensity in mixed silicate. As FTIR is not sensitive to Si-O symmetry stretching vibrations,[22,28] no noticeable changes with TiO_2 addition are observed in the width and depth of this broad band in the high-frequency region. Furthermore, it can be inferred that the band located at the intermediate-frequency region may likely originate from the Si-O-Ti asymmetric stretching vibrations and Si-O-Si symmetric stretching vibrations.[23,29] According to McMillan[30] and Virgo *et al.*,[31] the occurrence of the Si-O-Si peak was made possible by the symmetric stretching motion of the bridging oxygens (BOs) in Q^1 ($Si_2O^{6-}_7$). The transmittance through the Si-O-Si peak becomes deeper with increasing TiO_2 content, which implies that the BO content in the molten fluxes is increased. In addition, the band located at the low-frequency region is originated from the Si-O and Ti-O stretching vibrations,[15,25] and the Ti-O stretching vibrations become more pronounced due to the increased TiO_2 content.

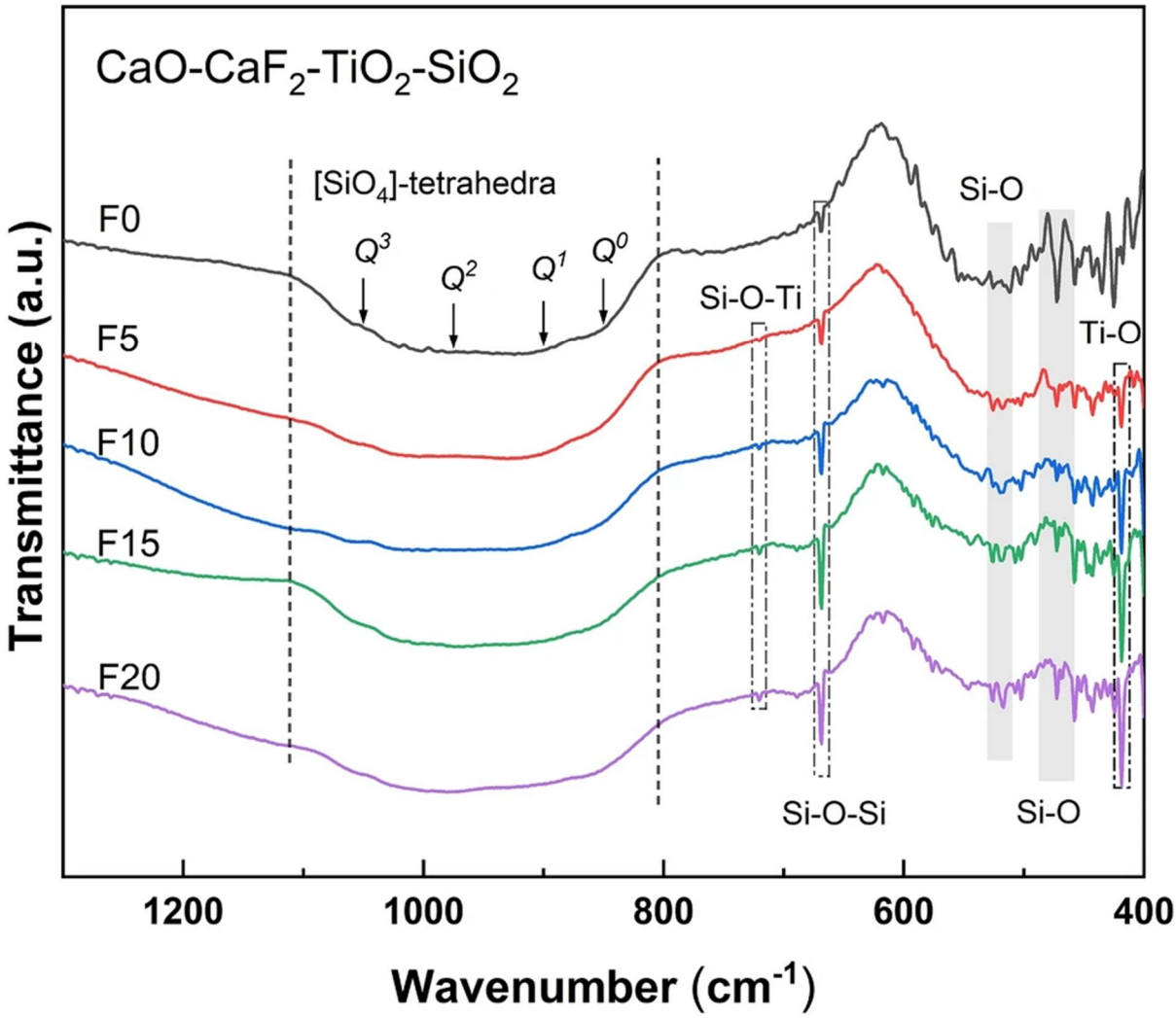

Fig. 2FTIR spectra of the fuesd flux samples

Raman spectroscopy, as shown in Figure 3, has been utilized to complement infrared spectroscopy for quantitative structural information revealing details of the $[SiO_4]$-tetrahedra units. Previous studies[21,32,33,34] indicated that the centers of the bands correlated to Q^4, Q^3, Q^2, Q^1 and Q^0 were located at ~1200, ~1040, ~970, ~910 and ~870 cm^{-1}, respectively. The centers of Ti-related bands associated with Ti-O stretching vibrations in $[Ti_2O_6]^{4-}$ chain units, Ti-O stretching vibrations in $[TiO_4]^{4-}$ monomers, and O-(Ti, Si)-O are located at ~840, ~790, and ~710 cm^{-1}, respectively.[15] As can be seen in Figure 3, the range of the characteristic peak is gradually extended from 800 to 600 cm^{-1} with the introduction TiO_2, and the relative intensity of Q^3 and Q^2 significantly decreases with increasing TiO_2 content. Alternatively, the intensity of $[Ti_2O_6]^{4-}$ and $[TiO_4]^{4-}$ bands increases as TiO_2 content is enhanced. All in all, the results from Raman spectra also suggest that the molten structure of the flux transforms from silicate to titanosilicate as TiO_2 content increases.

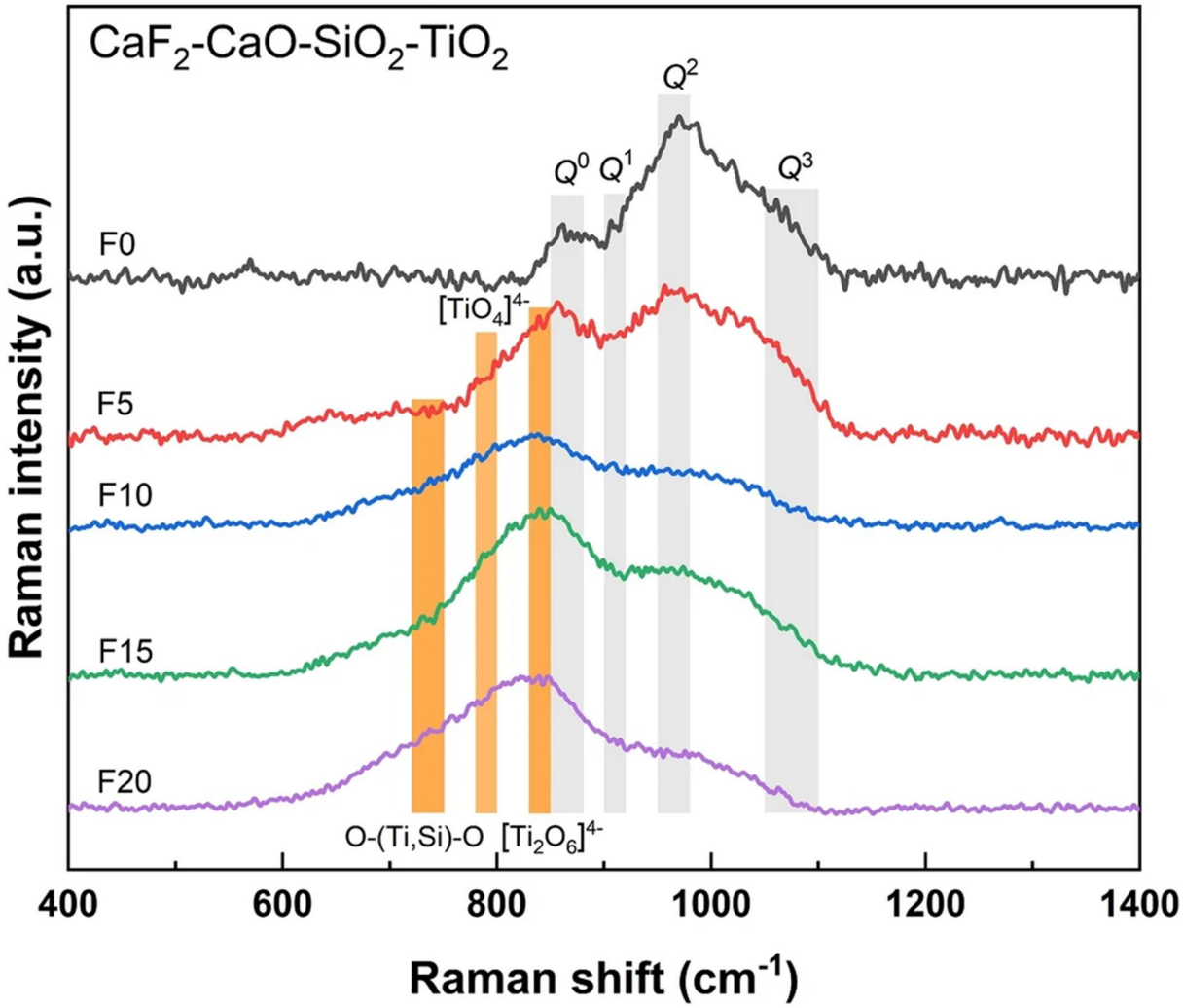

Fig. 3. Raman spectra of the fuesd flux samples

Various [TiO_t] and [SiO_4]-tetrahedra structural units overlap within a narrow range of frequencies. Therefore, Raman spectra have been fitted by assuming Gaussian line shapes for peaks of different structural units. The typical deconvolution results of the Raman spectra for TiO_2-free (F0) and TiO_2-contaiend (F10) samples are shown in Figures 4(a) and (b), respectively. The main bands of a TiO_2-free (F0) flux are associated with [SiO_4]-tetrahedra units, and the Ti-related bands appear with the introduction TiO_2, such as O-(Ti, Si)-O, $[TiO_4]^{4-}$, and $[Ti_2O_6]^{4-}$. Based on the band areas of the fitted curves, the area fractions of Ti-related units are shown in Figure 4(c). The area fractions of $[TiO_4]^{4-}$, $[Ti_2O_6]^{4-}$ and O-(Si, Ti)-O increase with increasing TiO_2 content. According to Hess *et al.*,[35] [TiO_t] structural units may exist as edge-sharing oligomers of self-connecting structures and corner-sharing oligomers connected with [SiO_4]-tetrahedra structures. Therefore, it is likely that simpler [TiO_t] structural units may replace more complex [SiO_4]-tetrahedra structures in the molten fluxes. The O-(Si, Ti)-O band indicates the structure of chain or sheet or a combination of both.[36] The O-(Ti, Si)-O linkages have been ushered into the flux structure by the introduction of Ti^{4+} into the silicate network, which is consistent with FTIR result that the intensity of Si-O-Ti asymmetric stretching vibrations slightly increases with increasing TiO_2 content. An additional parameter to characterize bond strength is field strength, which is defined as z/r^2, where z and r are the valence and radius of the cation, respectively. Field strength values of Ca^{2+}, Ti^{4+}, and Si^{4+} are 200.0, 1075.0 and 2500.0 nm^{-2}, respectively.[37]

When CaO is introduced into the melt, the filed strength of Ca^{2+} is significantly weaker than that of Si^{4+} and Ti^{4+}, so as to O^{2-} in CaO prefers to bond with Si^{4+} and Ti^{4+} to form $[SiO_4]$-tetrahedra and $[TiO_t]$ groups.[25] It is clear that there, indeed, exists a competitive relationship of O^{2-} between Si^{4+} and Ti^{4+}. Moreover, the relationship between concentrations of silicate and titanate structural units may be presented by reaction,[1,38] the Ti-O bonds in $[TiO_t]$ compete with silicate to coordinate Ca^{2+} so as to maintain local charge balance. Furthermore, according to the equilibrium constant for reaction,[1] in the slag at a given CaO/SiO_2 mass ratio, the reduction of the silicate units will facilitate the formation of $[Ti_2O_6]^{4-}$ and $[TiO_4]^{4-}$ units. Consequently, a few non-bridging oxygens (NBOs) linked to Si^{4+} turn into bridging oxygens (BOs), the gross polymerization of silicate network is enhanced by the increase of TiO_2.

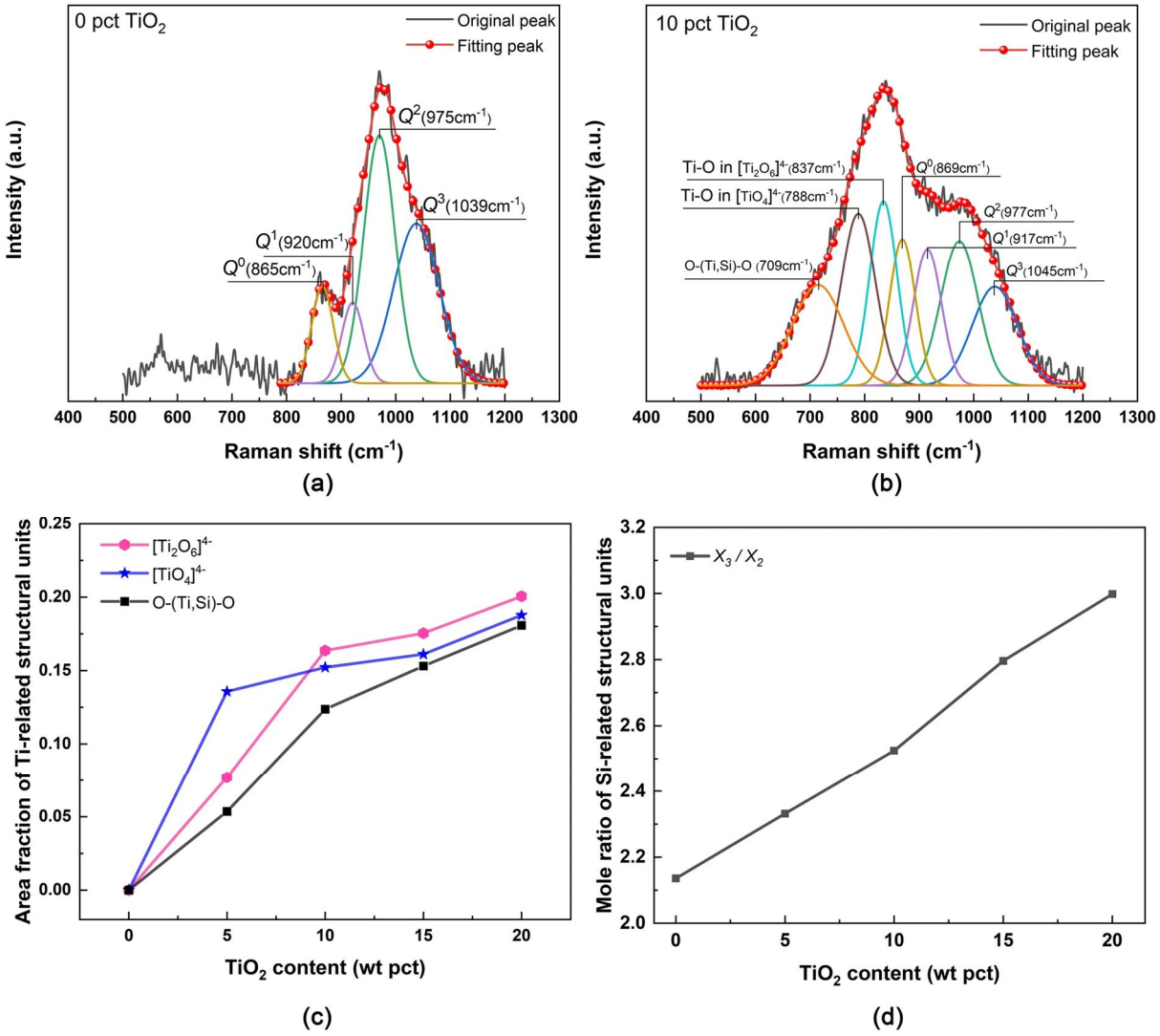

Fig. 4. (*a*) and (*b*) Typical deconvolution results of the Raman spectra for TiO_2-free (F0) and TiO_2-contaiend (F10) samples, (*c*) Area fraction of various Ti-related structural units, and (*d*) Mole ratios of Q^3 to Q^2 (X_3/X_2) as a function of TiO_2 content

$$(Si\text{-}O\text{-}Ca\text{-}O\text{-}Si)+(Ti\text{-}O\text{-}Ti)=(Ti\text{-}O\text{-}Ca\text{-}O\text{-}Ti)+(Si\text{-}O\text{-}Si) \quad (1)$$

To further prove that TiO_2 enhances the degree of polymerization (DOP) of silicate units, the X_3/X_2 (Q^3/Q^2 mole ratio) is introduced as the an index for the DOP of silicate units based on

the following equilibrium reaction among silicate units.[31,39] The X_3/X_2 is given by the following equation, [40,41] where A_i denotes band area of Q^i.

$$X_3/X_2=2.92(A_3/A_2) \quad (2)$$

As shown in Figure 4(d), the X_3/X_2 ratios monotonously increase with increasing TiO_2 content, indicating the enhanced DOP of the flux structure. Moreover, the increasing content of TiO_2 promotes. the competition between the Ti^{4+} and Si^{4+} for the limited O^{2-} supply from CaO, *i.e.*, more free oxygens O^{2-} are used to bond with Ti-related structures.

Figure 5(a) present typical deconvoluted peaks from O_{1s} XPS analysis of O^0 (BO), O^- (NBO), and O^{2-} (free oxygen) for F20. The full-width half-maximum (FWHM) of all fitted peaks is optimized to be less than 2.0 eV. The mole fraction of the individual oxygen anion species from the XPS spectra, which are obtained from the integrated area of the deconvoluted spectrum for each oxygen specie, is shown in Figure 5(b). As can be seen, the mole fraction of O^0 significantly increases with TiO_2 addition. Corresponding mole fraction of O^- decreases with higher TiO_2 content in the fluxes. According to Kim *et al.*,[6] the equilibrium distribution of O^0, O^-, and O^{2-} in molten fluxes can be expressed as:

$$2O^- \underset{\text{Depolymerization}}{\overset{\text{Polymerization}}{\rightleftarrows}} O^0 + O^{2-} \quad (3)$$

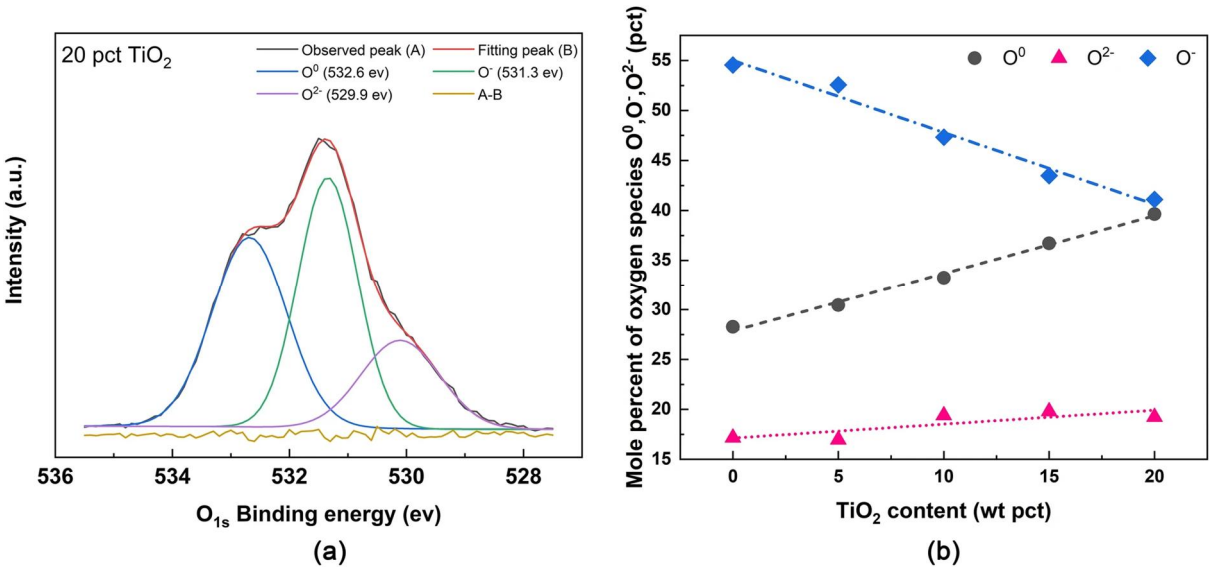

Fig. 5. (*a*) Typical deconvolution result of O_{1s} XPS spectra for F20; (*b*) Mole fraction of oxygen species

Ti^{4+} persists in the forms of $[Ti_2O_6]^{4-}$ and $[TiO_4]^{4-}$ in order to maintain charge balance, and these titanate units must compete with silicate units to coordinate Ca^{2+} cations. Hence, addition of TiO_2 to silicate melts causes some portion of the O^- in the silicate units to be transformed to O^0, promoting the depolymerization trend of the flux structure. It can be inferred that O^{2-} may have been consumed in the complex $[SiO_4]$-tetrahedra network and $[TiO_t]$. The increased O^0 and the lowered O^- may have been resulted from higher DOP, which is consistent with FTIR and Raman analysis.

Investigations by Zheng *et al*.[15] and Park *et al*.[42] shows that the viscosity and apparent activation energy of slags decrease with increasing TiO_2 content, which seemed to be inconsistent with the results of increasing DOP in present work. However, the field strength and electronegativity of Si were higher than those of Ti, and the strength of the Ti-O bond was weaker than the Si-O bond, which are 466 and 305 kJ/mol, respectively.[43] Thus, by substitution TiO_2 for some of SiO_2, a considerable proportion of $[TiO_4]^{4-}$ and $[Ti_2O_6]^{4-}$ may be introduced into the silicate network, leading to a higher DOP but weakening the strength of the silicate network. Moreover, Raman curves related to Ti indicate that a significant amount of simpler and smaller structural units, such as $[Ti_2O_6]^{4-}$ chains units and $[TiO_4]^{4-}$ monomers, have been brought into the slags by TiO_2 addition. Consequently, the incorporation of TiO_2 into molten slags could enhance the DOP of slag structure, and weaken the bond strength of $[SiO_4]$-tetrahedra network groups. Therefore, the viscosity and apparent activation energy for TiO_2-bearing slags both decrease with TiO_2 addition due to weaker Si-O bonds in the network and simpler units in the slags.

A brief summary of the structural roles of TiO_2 is given to explain the reason for the increase of DOP with increasing TiO_2 content. The FTIR results showed that the Si-O-Si peaks gradually increased, suggesting strengthened vibration between different Si-related tetrahedral units. In addition, the increasing Q^3/Q^2 mole ratios demonstrate the enhanced DOP of the slag system. The addition of TiO_2 promotes the competition between the Ti^{4+} and Si^{4+} for the limited O^{2-} supply from CaO. Moreover, to maintain local charge balance, a considerable amount of $[Ti_2O_6]^{4-}$ and $[TiO_4]^{4-}$ units compete with silicate, which leads to a few NBOs linked to Si^{4+} turn into BOs. Consequently, the gross polymerization of silicate network is enhanced by the increase of TiO_2.

In summary, amorphous fluxes derived from CaF_2-SiO_2-CaO-TiO_2 formula have been prepared. It was found that the Ti^{4+} mainly exists in form of $[Ti_2O_6]^{4-}$ and $[TiO_4]^{4-}$, and the flux structures gradually transform from silicate to titanosilicate system with increasing TiO_2 content. The introduction of Ti^{4+} into $[SiO_4]$-tetrahedra network plays the role of network-formers and yields a higher DOP for fluxes, which has been demonstrated by the increase in mole ratio of Q^3/Q^2 and mole fraction of O^0. TiO_2 also lowers the strength of the silicate network.

Acknowledgments

The authors sincerely thank the National Natural Science Foundation of China (Grant Nos. 51861130361, 51861145312, and 51850410522), Newton Advanced Fellowship by the Royal Society (Grant No. RP12G0414), Special Fund for Key Program of Science and Technology of Liaoning Province (Grant No. 2019JH1/101000014), Research Fund for Central Universities(Grant Nos. N172502004, and N2025025), Xingliao Talents Program (XLYC1807024 and XLYC1802024), and State Key Laboratory of Metal Material for Marine Equipment and Application (Project No. SKLMEA-K201903) for their financial support.

References

1. V. Sengupta, D. Havrylov and P. F. Mendez: *Weld. J.,* 2019, vol. 98, pp. 283s-313s.

2. C. A. Natalie and D. L. Olson: *Ann. Rev. Mater. Sci.,* 1986, vol. 16, pp. 389-413.

3. V. Sengupta and P. F. Mendez: *Weld. J.*, 2017, vol. 96, pp. 334s-53s.

4. S.H. Sui, W.W. Cai, Z.Q. Liu, T.G. Song and A. Zhang: *J. Iron Steel Res. Int.*, 2006, vol. 13, pp. 65-68.

5. J.B. Kim and I. Sohn: *ISIJ Int.*, 2014, vol. 54, pp. 657-63.

6. J.B. Kim, T.H. Lee and I. Sohn: *Metall. Mater. Trans. A*, 2018, vol. 49A, pp. 2705-20.

7. C. B. Dallam, S. Liu and D. L. Olson: *Weld. J.*, 1985, vol. 64, pp. 140s-51s.

8. L. Sharma and R. Chhibber: *Silicon*, 2019, vol. 11, pp. 2763-73.

9. J. Zhang, J. Leng and C. Wang: *Metall. Mater. Trans. B*, 2019, vol. 50, pp. 2083-87.

10. J. Roy, R. N. Rai and S. C. Saha: *J. Mater. Process. Tech.*, 2018, vol. 56, pp. 313-25.

11. B. Deepak, C. Rahul, A. Navneet and M. Rajeev: *J. Manuf. Process.*, 2016, vol. 23, pp. 61-74.

12. A. M. Paniagua-Mercado, V. M. Lopez-Hirata, H. J. Dorantes-Rosales, P. E. Diaz and E. D. Valdez: *Mater. Charact.*, 2009, vol. 60, pp. 36-39.

13. I. Sohn, W. Wang, H. Matsuura, F. Tsukihashi and D. J. Min: *ISIJ Int.*, 2012, vol. 52, pp. 158-60.

14. A. Shankar, M. Görnerup, A. K. Lahiri and S. Seetharaman: *Metall. Mater. Trans. B*, 2007, vol. 38, pp. 911-15.

15. K. Zheng, Z.T. Zhang, L.L. Liu and X.D. Wang: *Metall. Mater. Trans. B*, 2014, vol. 45, pp. 1389-97.

16. J. Zhang, T. Coetsee and C. Wang: *Metall. Mater. Trans. B*, 2020, vol. 51, pp. 16-21.

17. T. Gabriella, O. Ostrovski and S. Jahanshahi: *Metall. Mater. Trans. B*, 2002, vol. 33, pp. 61-67.

18. S. Yu, S. Liu, M. Xie, Z. Li and J. Wang: *Acta Metall. Sin.*, 1998, vol. 34, pp. 91-94.

19. D. D. Schwemmer, D. L. Olson and D. L. Williamson: *Weld. J.*, 1979, vol. 58, pp. 153s-60s.

20. J. H. Park, D. J. Min and H. S. Song: *ISIJ Int.*, 2002, vol. 42, pp. 38-43.

21. G. H. Kim, C. S. Kim and I. Sohn: *ISIJ Int.*, 2013, vol. 53, pp. 170-76.

22. Z. Chen, H. Wang, Y. Sun, L. Liu and X. Wang: *Metall. Mater. Trans. B*, 2019, vol. 50, pp. 2930-41.

23. J. B. Kim and I. Sohn: *J. Non-Cryst. Solids*, 2013, vol. 379, pp. 235-43.

24. J. H. Park: *ISIJ Int.*, 2012, vol. 52, pp. 1627-36.

25. S. Seetharaman, A. McLean, R. Guthrie and S. Sridhar: *Treatise on Process Metallurgy*, 1st ed., Elsevier, Oxford, 2013, pp. 149-286.

26. X. Shen, M. Chen, N. Wang and D. Wang: *ISIJ Int.,* 2019, vol. 59, pp. 9-15.

27. C. Feng, J. Tang, L.H. Gao, Z.G. Liu and M.S. Chu: *ISIJ Int.*, 2019, vol. 59, pp. 31-38.

28. B. N. Roy: *J. Am. Ceram. Soc*., 1990, vol. 73, pp. 846-55.

29. A. Murashkevich, A. Lavitskaya, T. Barannikova and I. Zharskii: *J. Appl. Spectrosc.* 2008, vol. 75, pp. 730-34.

30. P. McMillan: *Am. Mineral.,* 1984, vol. 69, pp. 645-59.

31. D. Virgo, B. O. Mysen and I. Kushiro: *Science,* 1980, vol. 208, pp. 1371-73.

32. Y.Q. Sun, H. Wang and Z.T. Zhang: *Metall. Mater. Trans. B,* 2018, vol. 49, pp. 677-87.

33. G. H. Kim and I. Sohn: *J. Non-Cryst. Solids,* 2012, vol. 358, pp. 1530-37.

34. Z. Wang, Y. Sun, S. Sridhar, M. Zhang, M. Guo and Z. Zhang: *Metall. Mater. Trans. B,* 2015, vol. 46, pp. 537-41.

35. N. J. Hess, Y. Su and M. L. Balmer: *J. Phys. Chem. B,* 2001, vol. 105, pp. 6805-11.

36. B. O. Mysen, D. Virgo and C. M. Scarfe: *Am. Mineral.,* 1980, vol. 65, pp. 690-710.

37. I. Sohn and D. J. Min: *Steel Res. Int.,* 2012, vol. 83, pp. 611-30.

38. B. O. Mysen, F. J. Ryerson and D. Virgo: *Am. Mineral.,* 1980, vol. 65, p. 1150–65.

39. B. Mysen: *Eur. J. Mineral.,* 2003, vol. 15, pp. 781-802.

40. J. D. Frantza and B. O. Mysen: *Chem. Geol.,* 1995, vol. 121, pp. 155-76.

41. B. O. Mysen and J. D. Frantz: *Contrib. Mineral. Petrol.,* 1994, vol. 117, pp. 1-14.

42. H. Park, J. Y. Park, G. H. Kim and I. Sohn: *Steel Res. Int.,* 2012, vol. 83, pp. 150-56.

43. M. Weller, T. Overton, J. Rourke, F. Armstrong and P. Atkin: *Inorganic Chemistry*, 6th ed., Oxford University Press, Oxford, 2014, pp. 422-551.